Eur Biophys J (1993) 21, 369–383

European Biophysics Journal

Ion channel formation by zervamicin-IIB

A molecular modelling study

M. S. P. Sansom [1], P. Balaram [2], I. L. Karle [3]

[1] Laboratory of Molecular Biophysics, The Rex Richards Building, University of Oxford, South Parks Road, Oxford, OX1 3QU, UK
[2] Molecular Biophysics Unit, Indian Institute of Science, Bangalore 560 012, India
[3] Laboratory for the Structure of Matter, Naval Research Laboratory, Washington D.C. 20375-5000, USA

Received: 21 August 1992 / Accepted in revised form: 29 September 1992

Abstract. Zervamicin-IIB (Zrv-IIB) is a 16 residue peptaibol which forms voltage-activated, multiple conductance level channels in planar lipid bilayers. A molecular model of Zrv-IIB channels is presented. The structure of monomeric Zrv-IIB is based upon the crystal structure of Zervamicin-Leu. The helical backbone is kinked by a hydroxyproline residue at position 10. Zrv-IIB channels are modelled as helix bundles of from 4 to 8 parallel helices surrounding a central pore. The monomers are packed with their C-terminal helical segments in close contact, and the bundles are stabilized by hydrogen bonds between glutamine 11 and hydroxyproline 10 of adjacent helices. Interaction energy profiles for movement of three different probes species (K^+, Cl^- and water) through the central pore are analyzed. The conformations of: (a) the sidechain of glutamine 3; (b) the hydroxyl group of hydroxyproline 10; and (c) the C-terminal hydroxyl group are "optimized" in order to maximize favourable interactions between the channel and the probes, resulting in favourable interaction energy profiles for all three. This suggests that conformational flexibility of polar sidechains enables the channel lining to mimic an aqueous environment.

Key words: Ion channel – Peptaibol – Molecular modelling – Channel-forming peptide

Introduction

The past decade has witnessed a substantial increase in interest in the molecular properties of receptor-gated ion channels, concomitant with an expansion of the sequence database for these multi-subunit, trans-membrane proteins. A low resolution image of the structure of the prototypic member of this superfamily, the nicotinic acetylcholine receptor, has been obtained by e.g. Toyoshima and Unwin (1990) using cryoelectron microscopy. Unfortunately, it has not proved possible to obtain atomic resolution structural information. However, insights into the molecular nature of the central pore region of channel proteins have been gained from studying simple model systems, namely channel forming peptides (CFPs; Sansom 1991).

CFPs are short (ca. 20 residues) hydrophobic peptides which adopt an α-helical conformation in the presence of lipid bilayers. Trans-membrane voltages induce them to form ion channels in bilayers, of comparable functional properties (conductance, ion selectivity etc.) to those of channel proteins. Channels are formed by a process of self-assembly within the plane of the bilayer which generates bundles of parallel trans-membrane helices. These helices surround a central pore, which is lined by hydrophilic sidechains, thus permitting permeation of selected ions. One reason for studying CFPs is that it is possible to relate their functional (i.e. electrical) properties to structural (NMR and/or X-ray diffraction) information in order to develop molecular models of channel structure.

The peptaibols are a family of channel-forming peptides which contain a high percentage of the helix-promoting residue α-aminoisobutyric acid (Aib). Each peptaibol molecule contains at least one proline residue, and the C-terminus is usually an α-amino alcohol e.g. phenylalaninol. The most intensively studied peptaibol is alamethicin (Alm; Mathew and Balaram 1983; Hall et al. 1984; Boheim et al. 1987), a 20 residue CFP. More recently, investigations have been extended to the zervamicins (Zrv), a family of 16 residue peptaibols isolated from *Emericellopsis salmosynnemata* (Rinehart et al. 1981; Krishna et al. 1990).

The channel-forming properties of zervamicin-IIB (Zrv-IIB) have been studied in some detail, (Agarwalla et al. 1992; Balaram et al. 1992). Channels are believed to be formed by parallel bundles of Zrv-IIB helices surrounding a central ion-permeable pore. Zrv-IIB has been shown to form multiple conductance level channels. The different conductance levels correspond to different numbers of monomers per bundle (N). The sequence of

Correspondence to: M. S. P. Sansom

Zrv-IIB is:

Ac-W-I-Q-J-I-T-U-L-U-O-Q-U-O-U-P-F-OH

where U = α-aminoisobutyric acid, O = hydroxyproline, J = (R)-isovaline and F-OH is the C-terminal phenylalaninol. The crystal structure of a closely related species, Zrv-Leu (which differs from Zrv-IIB only in that residue 1 is leucine rather than tryptophan; Karle et al. 1991), reveals the molecule to be largely helical, with a central kink introduced by the hydroxyproline at position 10. Previous modelling studies have suggested that such proline-induced kinks may provide cation binding sites in ion channels (Sansom 1992a). In this paper the structure of Zrv-Leu is used to model the structure of Zrv-IIB, which in turn is used to develop molecular models of Zrv-IIB channels. Zrv-IIB is an attractive candidate for modelling studies as it does not contain any ionizable sidechains. This avoids the problems of calculation of local pK_As when such sidechains are in relatively close proximity within intramembraneous helix bundles. A preliminary account of some of this work has appeared in abstract form (Sansom 1992c).

Methods

Helix bundles

All modelling was performed using QUANTA 3.2 (Polygen, Waltham, MA), run on a Silicon Graphics (Mountain View, CA) Indigo workstation. Molecular mechanics calculations were carried out using CHARMM (Brooks et al. 1983). Molecular structures were drawn using MolScript (Kraulis 1991). All auxiliary programs were written in Fortran77.

Helix bundles are generated using *bndlq*, as described in previous publications (Sansom et al. 1991; Sansom 1992a, b). Bundles are aligned such that the central pore axis is coincident with the z axis. Looking down z such that the N-termini are towards the viewer, the helices are named A, B, ... in an anticlockwise manner. Thus e.g. Oγ:10 (A) refers to the Oγ atom of residue 10 in helix A.

Hydrophilic surfaces

In constructing helix bundle models the first step is definition of the hydrophilic face of an amphipathic helix. This is done via empirical energy function calculation of the interaction of a water molecule with the surface of the helix. The oxygen atom of a water molecule is placed at successive positions, (z, r, ϕ), on a cylindrical polar grid. The z-axis of the grid is coincident with the helix axis. For each position of the water molecule, an energy minimization is performed in which peptide atoms and water oxygen atom are fixed whereas the water hydrogen atoms are free to move, thus generating an optimum orientation of the water molecule. The peptide-water interaction energy is then evaluated as the sum of a van der Waals and an electrostatic term, generating an array containing the interaction energy at each grid point, $E(z, r, \phi)$. For each value of (z, ϕ) the minimum value of E with respect to r is selected. The resultant $E_{min}(z, \phi)$ array is displayed as a contour plot, thus revealing the hydrophilic surface of the helix. A secondary plot is obtained by averaging E_{min} over z to yield $\langle E \rangle$. The minimum in a graph of $\langle E \rangle$ vs. ϕ thus defines the centre of the hydrophilic face of the helix, which is in turn used to determine orientation of the helix within a bundle. A more detailed exposition of this procedure and of its application to non-peptaibol CFPs is the subject of a forthcoming paper (Kerr and Sansom 1992).

Interaction energy profiles

Channel-ion interaction energy profiles were evaluated as in previous papers (Sansom et al. 1991; Sansom 1992a, b). The aim of these calculations is to probe for ion-liganding sites within the pore defined by a helix bundle. They do not estimate permeation profiles for ions moving through the pore, as the models do not include water and so fail to take into account solvation/desolvation energies of the ion. However, the results are of value in that they enable one to focus on possible ion-protein interactions within the bilayer region.

In these calculations, the channel model is treated as a rigid body. Polar hydrogen atoms are explicitly included, whereas non-polar hydrogens are included via an extended atom representation. The ion probe is placed at points along the z-axis. The empirical energy of interaction between ion and channel is evaluated as the sum of a van der Waals and an electrostatic term. In calculating the electrostatic energy a distance dependent dielectric is employed in order to mimic the effect of solvent-screening on channel-ion interactions at moderate separations. This method of probing the channel for potential liganding sites is related to the GRID program of Goodford (1985) and to the method of Furois-Corbin and Pullman (1986).

Ion-channel interaction energies are evaluated as the difference between the energy with the ion at a given point and the energy when ion and channel are separated by a considerable distance (typically ≥ 5.0 nm). Energy profiles are generated by translating the ion along the pore (i.e. z) axis, the interaction energy being evaluated as a function of z.

A similar method has been used to probe channel-water interactions. In these calculations the oxygen atom of a water molecule is placed at successive positions along z, and the optimum orientation determined in the same manner as described above for hydrophilic surface evaluations. The channel-water interaction energy is evaluated as the difference between the energy with the water at a given value of z and at $z \geq 5.0$ nm.

Results

Monomer structure

The structure of monomeric Zrv-IIB was modelled using the crystal structure of Zrv-Leu (Karle et al. 1991). The leucine residue at position 1 was replaced by a tryptophan

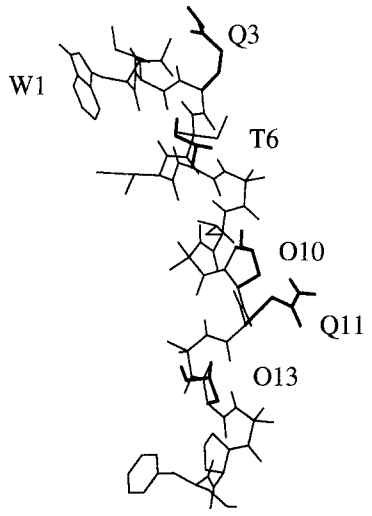

Fig. 1. Structure of a Zrv-IIB monomer, based on the crystal structure of Zrv-Leu. Sidechains making up the hydrophilic face of the Zrv-IIB monomer are highlighted using bold lines – glutamine at positions 3 and 11 (Q3 and Q11), threonine at position 6 (T6), and hydroxyproline at 10 and 13 (O10 and O13). Note the tryptophan ring at position 1 (W1) which replaces a leucine in this position in Zrv-Leu

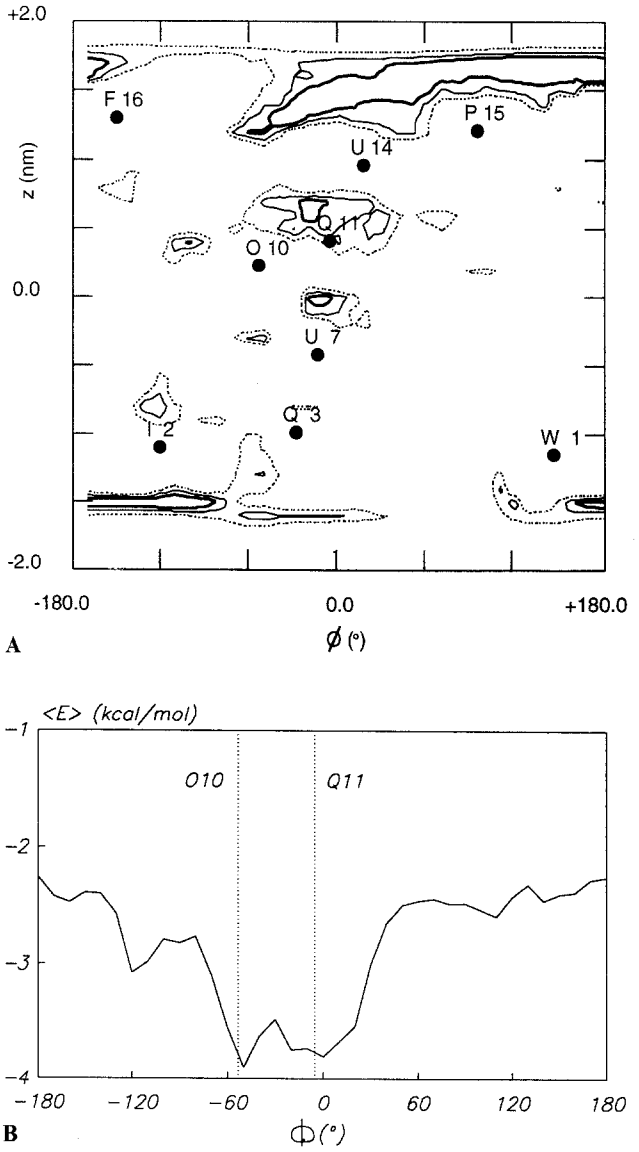

Fig. 2. (**A**) Hydrophilic surface map of the Zrv-IIB monomer. A contour plot of the interaction energy of a water molecule with the surface of Zrv-IIB is superimposed on the positions of Cα atoms of selected residues. The contour levels are −8 (thick lines), −6 (thin lines) and −4 (broken lines) kcal/mol. (**B**) Secondary plot, derived from (**A**), of the average interaction energy $\langle E \rangle$ vs. ϕ. The two minima in the curve, at $\phi = -50°$ and 0°, correspond to the positions, on ϕ, of the Cα atoms of residues O10 and Q11 respectively (as indicated by the vertical dotted lines)

(W1). The orientation of the W1 sidechain was optimized by a grid search about torsion angles χ_1 (N-Cα-Cβ-Cγ) and χ_2 (Cα-Cβ-Cγ-Cδ2) in order to determine the minimum energy conformation. The model was then subjected to 50 cycles of unrestrained steepest descents energy minimization in order to reconcile any minor stereochemical conflicts. The resultant structure is shown in Fig. 1. The conformation of the sidechain of W1 is defined by $\chi_1 = -62.5°$ and $\chi_2 = -60.4°$, which is close to a preferred conformation of tryptophan (Janin et al. 1978) in which $\chi_1 = -60°$ and $\chi_2 = -90°$. This conformation of W1 is such that the Nε1-H bond is approximately parallel to the axis of the N-terminal helix, pointing away from the centre of the peptide molecule. As will be seen, in the channel model this results in this potential hydrogen-bond donor being positioned such that it would point towards the bilayer interface, whilst the remainder of the aromatic sidechain would be located within the hydrophilic region of the bilayer. Such an orientation of tryptophan sidechains may be a general feature of membrane proteins (Schiffer et al. 1992).

The Zrv-IIB molecule is amphipathic i.e. it has a hydrophobic and a hydrophilic face. The total solvent accessible surface area of Zrv-IIB is 19.9 nm^2. Of this, ca. 12% is made up of polar groups. Examination of the structure of the monomer (Fig. 1) suggests that the main sidechains defining the hydrophilic, convex face of the molecule are Q3, T6, O10, Q11 and O13. The hydrophilic surface of Zrv-IIB may be delineated more precisely by calculation of a hydrophilic surface map. Helix-water interaction energies are displayed on a contour plot as a function of (z, ϕ), where z is distance along the helix axis and ϕ is the angle of rotation about this axis. For this calculation, the helix axis was defined as running from the midpoint of Cα:1–4 to the midpoint of Cα:13–16. In Fig. 2A $z = +2$ nm corresponds to the C-terminus and $z = -2$ nm corresponds to the N-terminus. The positions, on (z, ϕ), of the Cα atoms of selected residues are also shown. From this plot, three distinct regions of interaction of water molecules with Zrv-IIB may be seen. Two of these are at the N- and C-termini, where favourable interactions are seen for a wide range of values of ϕ. At the N-terminus this corresponds to water interactions with the Nε1-H group of W1, with the amide N-H groups of residues 1 to 3 and, to a lesser extent, with the amide group of the Q3 sidechain. At the C-terminus water may interact favourably with the carbonyl oxygens of residues 14 and 15, and with the terminal (F16-OH) hydroxyl

group. In between these two "bands" of hydrophilic groups, there is a cluster of favourable water interactions close to the centre, on z, of the molecule, in the region of $\phi = 0°$. Three groups appear to be responsible for this. The carbonyl oxygen of residue 7 is exposed to solvent by the (hydroxy)proline induced-kink in the helix (Fox and Richards 1982; Sansom 1992a). This generates a region of favourable solvent interaction close to $z = 0$ nm. The sidechain hydroxyl of O10 and the sidechain amide of Q11 generate a region of strongly favourable water interactions, centred about $z \approx +0.5$ nm and $\phi \approx -30°$. Thus the overall hydrophilic surface is approximately hourglass-shaped, with a narrow strip of favourable interactions linking two bands at either end of the peptide. This feature is seen in a range of channel-forming peptides (Kerr and Sansom 1992).

The corresponding secondary plot, of $\langle E \rangle$ vs. ϕ, is shown in Fig. 2B. There are two minima, of approximately equal $\langle E \rangle$ values. One, at $\phi = 0°$, corresponds to the position on ϕ of the Cα of Q11. The other, at $\phi = -50°$ corresponds to O10. Thus, there are two alternative definitions of the centre of the hydrophilic face of the Zrv-IIB molecule. Consequently two possible values of θ were explored in helix bundle model building using *bndlq*. Notice that even for $\phi = 180°$ $\langle E \rangle$ is negative. This is because of the two "bands" of hydrophilic interactions at either end of the Zrv-IIB molecule, at which favourable interactions are possible for (nearly) all ϕ values.

Helix bundles

The geometry of a parallel helix bundle may be defined by four parameters: (a) the angle between the helix axis and the z-axis, this being of particular importance when kinked helices, as in the peptaibols, are involved; (b) the angle of rotation, θ, of the monomer about the z-axis, which defines the orientation of the hydrophilic face with respect to the centre of the pore; (c) the distance between the centres of the helix axes of adjacent monomers, R; and (d) the number, N, of helices per bundle.

In an earlier study of a synthetic apolar zervamicin, Zrv-A1-16 (Sansom et al. 1991) a channel model was proposed in which the C-terminal helical segments formed a close-packed, parallel bundle. This model was used as the basis of a preliminary model of Zrv-IIB (Balaram et al. 1992; Sansom 1992c) in which the monomers were oriented such that the sidechains of Q11 were directed towards the centre of the pore. This Zrv-IIB channel model thus corresponded to monomer alignment using the minimum at $\phi = 0°$ in the $\langle E \rangle$ vs. ϕ graph to define the θ value in *bndlq*, resulting in a similar value of θ to that used in the Zrv-A1-16 channel model. In the latter case the helix orientation was dictated by the need to direct the only hydrophilic region, i.e. the exposed carbonyl oxygen of residue 7, towards the centre of the pore. Note that in all models of peptaibol channels the helices are aligned approximately parallel to one another, rather than in an anti-parallel manner. This is in order to be consistent with current theories of peptaibol channel formation, in which the helix dipoles (Hol et al. 1978) reorient in response to an imposed transbilayer potential forming parallel bundles (Sansom 1991).

In the current study several alternative models were explored. For example, models with the C-terminal and the N-terminal helical segments close packed have been compared. Of these, the former allow closer packing with fewer stereochemical conflicts and thus have been selected for further investigation. Exploration of models in which θ was varied resulted in a more favourable geometry than that employed in the preliminary Zrv-IIB channel model described above. In this revised model, the hydroxyl groups of O10, rather than the Q11 sidechains, are directed towards the central pore. This corresponds to defining θ using the minimum at $\phi = -50°$ in the $\langle E \rangle$ vs. ϕ curve. This adjustment brings about more favourable inter-monomer interactions (see below). Furthermore, adjustment of sidechain conformations was *not* required for close packing of helices, whereas in the previous model it was necessary to adjust the conformations of V6 and L8. The revised model was therefore the basis for all further calculations. It was subjected to 50 cycles of energy minimization to remove any minor stereochemical conflicts.

The overall geometry of the revised model of an $N = 6$ Zrv-IIB helix bundle is shown in Fig. 3A. The helix-helix separation was 0.95 nm. As can be seen the orientation of the helices is such that sidechains Q3 and O10 (shown in monomer conformation *B* – see below) are directed towards the centre of the pore. Two opposite monomers (A and D) from the same model viewed down the y-axis, i.e. perpendicular to the central pore axis, are shown in Fig. 3B. It is evident that Q3 and O10 form the hydrophilic lining of the pore. The wider mouth of the pore corresponds to the N-termini of the monomers, whereas the narrower mouth of the pore corresponds to the C-termini. For example, in the $N = 6$ bundle the Oε1:3(A) to Oε1:3(D) separation, i.e. the closest distance between opposite monomers at the N-terminal mouth of the pore, is 1.64 nm. The pore narrows in the middle (the Oγ:10(A) to Oγ:10(D) separation is 1.13 nm), the then widens somewhat towards the C-terminus, with an O:16(A)-O:16(D) separation of 1.54 nm. The minimum diameter of the pore is defined by the Cβ atoms of O:10 as $d_{min} = 2\,[r\,(C\beta{:}10) - 0.217]$ nm, where r (Cβ:10) is the distance from the centre of the pore to that of the Cβ:10 atom, and 0.217 nm is the (extended) radius of the Cβ atom. Thus, for $N = 4$ to 8, $d_{min} = 0.25, 0.44, 0.71, 1.01$ and 1.30 nm respectively.

An important feature of this model is that it provides a structural explanation for the existence of multiple conductance level Zrv-IIB channels. As described in an earlier paper (Balaram et al. 1992) multiple conductance levels may be explained in terms of helix bundles with differing values of N. Conductance data suggest that cyclindrically symmetrical bundles are formed for $N = 4, \ldots, 8$. Accordingly, helix bundle models with $N = 4, \ldots, 8$ monomers/bundle have been constructed (that for $N = 4$ has a greater helix-helix separation than the others, all of which have $R = 0.95$ nm – see below). In all of these models an inter-monomer hydrogen bond is formed, from Hγ of O13(B) to Oε1 of Q11(A) (and between corresponding symmetry

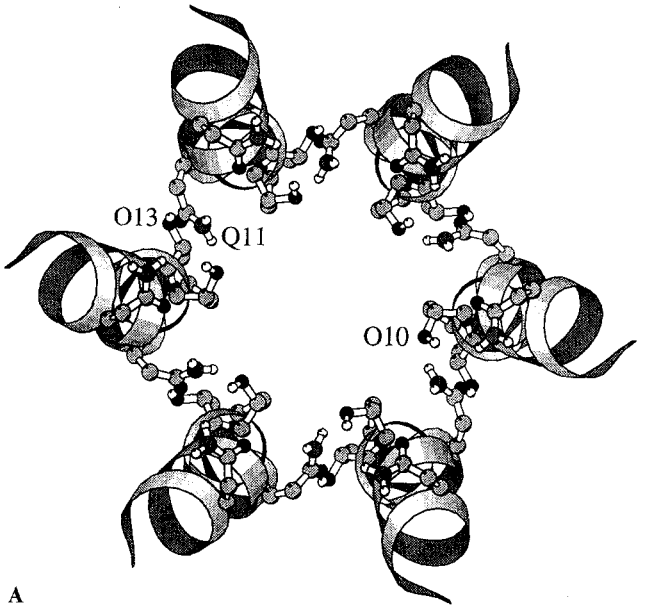

A

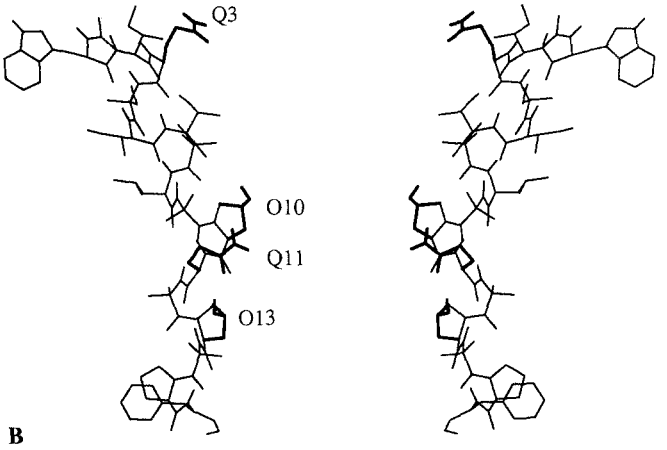

B

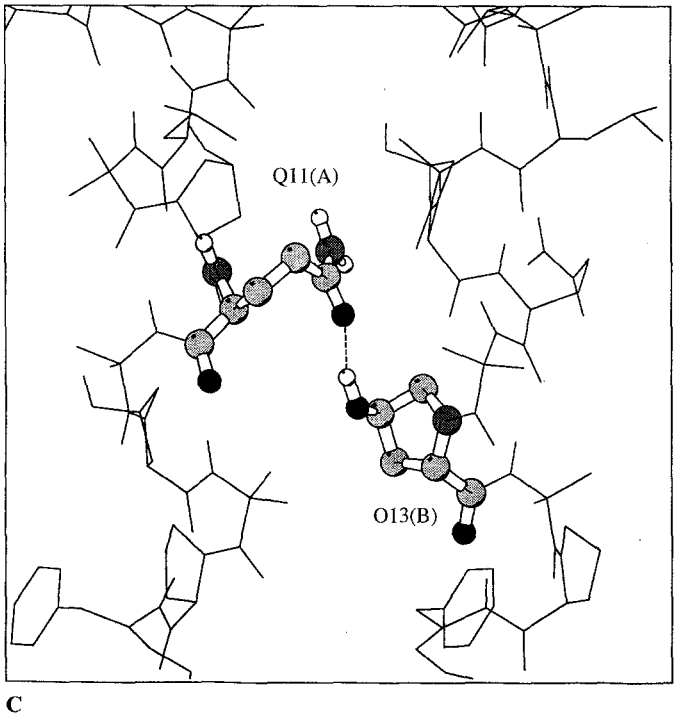

C

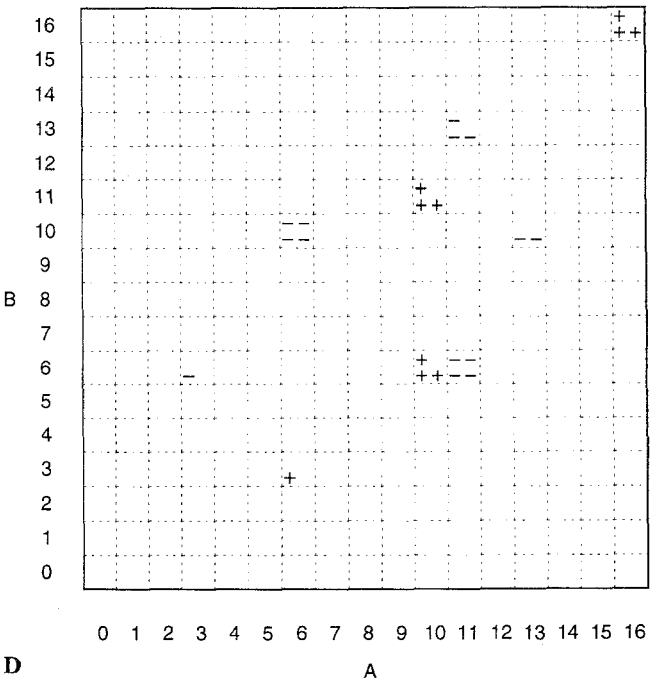

D

Fig. 3A–D. An $N=6$ helix bundle model of a Zrv-IIB channel. The monomers are in conformation B, as defined in the text and in the legend to Fig. 5. (**A**) is a schematic diagram of the helix bundle, viewed down the pore axis (i.e. the z axis). The peptide backbone is shown as a ribbon. The sidechains of the main hydrophilic residues, Q3 (not labelled), O10, Q11 and O13 are shown. (**B**) presents a view of the same model, looking down the x-axis at two opposite monomers (A and D). The four polar sidechains are highlighted. (**C**) shows the inter-monomer hydrogen bond from the hydroxyl group of O13(B) to the amide oxygen of the sidechain of Q11(A). The view is down a perpendicular to the monomer A-monomer B interface. (**D**) Inter-helix charge-charge contact map for interactions at the monomer-monomer interface shown in (**C**). The elements of the array correspond to the interaction energy of sidechain i in monomer A with sidechain j in monomer B. These energies are indicated as follows: $++++ \geq +8$ kcal/mol; $+++ \geq +6$ kcal/mol; $++ \geq +4$ kcal/mol; $+ \geq +2$ kcal/mol; $- \leq -2$ kcal/mol; $-- \leq -4$ kcal/mol; $--- \leq -6$ kcal/mol; and $---- \leq -8$ kcal/mol

related pairs). The geometry of this hydrogen bond, for the $N=6$ model, is illustrated in Fig. 3C. The amide group of the Q11(A) sidechain fits into a pocket between the hydroxyl groups of O10(B) and O13(B), with the latter acting as a hydrogen bond donor to the amide oxygen atom. The hydrogen bond is aligned approximately parallel (i.e. at an angle of 12.3°) to the z-axis. Consequently, variations in N do not greatly alter the hydrogen bonding geometry, as summarised in Table 1. In particular, neither the H · · · O distance nor the O–Ĥ · · · O angle is strongly dependent upon N. Averaging over N the mean value of the H · · · O distance is 1.98 (±0.05) Å and the mean O–Ĥ · · · O angle is 156 (±5)°. These values compare reasonably well with those for comparable hydrogen bonds obtained by high resolution neutron diffraction studies (Jeffrey and Saenger 1991). These observations are important in that they suggest that bundle stabilization is relatively insensitive to changes in N, in agreement with the existence of multiple conductance levels for Zrv-IIB channels.

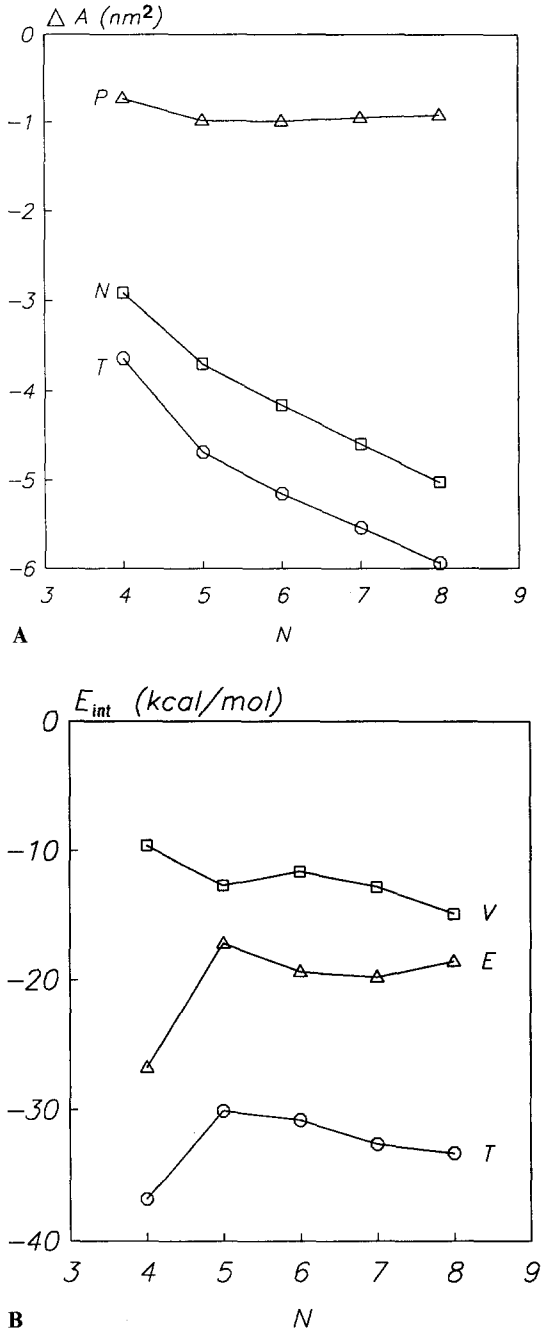

Fig. 4. (**A**) Buried surface areas for $N=4,\ldots,8$ helix bundles. The change in solvent accessible surface area per monomer upon helix bundle formation (ΔA) is shown as a function of N. Changes in surface area for polar (P), non-polar (N) and the total for all atoms (T) are shown. (**B**) Monomer-monomer interaction energies (E_{int}) for the same helix bundles. The van der Waals (V) and electrostatic (E) components of the total interaction energy (T) per monomer-monomer interface are shown

Analysis of inter-helix charge-charge contact maps (Fig. 3D; Nilges and Brünger 1991) suggests that the following electrostatic interactions between sidechains stabilize the monomer-A:monomer-B interface in the $N=6$ model: T6(A)-O10(B); Q11(A)-T6(B); Q11(A)-O13(B); and O13(A)-O10(B). Thus interactions between polar sidechains seem to be of general importance in stabilization of Zrv-IIB helix bundles.

Table 1. Inter-monomer hydrogen bond geometry

N	d(Oγ:13(B)–Oε:11(A))/Å	d(Hγ:13(B)–Oε:11(A))/Å	θ(Oγ:13(B)–Hγ:13(B)–Oε:11(A))/°
4	2.92	1.98	164
5	2.84	1.92	160
6	2.82	1.93	152
7	2.87	1.99	150
8	2.96	2.07	153

Monomer-monomer interactions as a function of N have been evaluated in two ways – via evaluation of changes in accessible surface area, and via calculation of interaction energies. Figure 4A shows changes in accessible surface area per monomer upon bundle formation as a function of N, calculated using a 0.14 nm diameter probe. The total change in area is broken down into contributions from polar and from non-polar atoms. It can be seen that the change in polar surface area is almost independent of N, whereas the area of the non-polar surface buried increases as N increases. The interaction energy at the monomer-monomer interface was calculated as $E_{int}=E_{dimer}-2E_{monomer}$. This interaction energy is shown as a function of N in Fig. 4B. It is evident that the van der Waals component of E_{int} decreases somewhat as N increases. Apart from the step from $N=4$ to $N=5$ (see below), the electrostatic component of the interaction energy (which includes the hydrogen bonding energy) is approximately independent of N. Thus, both types of analysis suggest that inter-monomer electrostatic interactions, including hydrogen bonding, provide an approximately constant contribution to the stabilization of helix bundles for $N=4,\ldots,8$.

Sidechain conformations

In the Zrv-IIB monomer, sidechain conformations were the same as those present in the Zrv-Leu crystal structure. However, sidechain conformations may change, to a limited extent, when Zrv-IIB monomers form a helix bundle, and when ions pass through the resultant channel. Indeed, the possibility of sidechain conformational changes in relation to channel gating was discussed in the initial communication of the crystal structure of Zrv-Leu (Karle et al. 1991). Also, sidechain conformational changes in relation to transient ion binding sites have been investigated in the context of models of nicotinic acetylcholine receptors and related channels (Sansom 1992b). Consequently, possible changes in sidechain conformations in Zrv-IIB models have been explored.

The method used to explore sidechain conformational changes was similar to that described in Sansom (1992b). An ion was placed on the z-axis adjacent to a monomer from a Zrv-IIB helix bundle. The ion was placed, successively, adjacent to the sidechain of Q3, to the hydroxyl group of O10 and to the C-terminal hydroxyl group. With a K^+ ion next to Q3, a conformational search about $\chi_2=C\alpha-C\beta-C\gamma-C\delta$ and $\chi_3=C\beta-C\gamma-C\delta-O\varepsilon$ of the

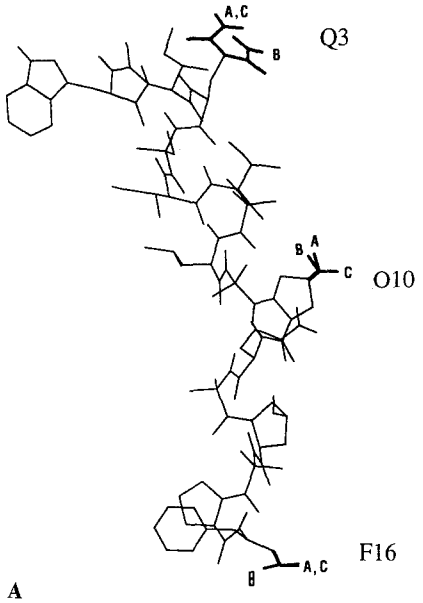

A

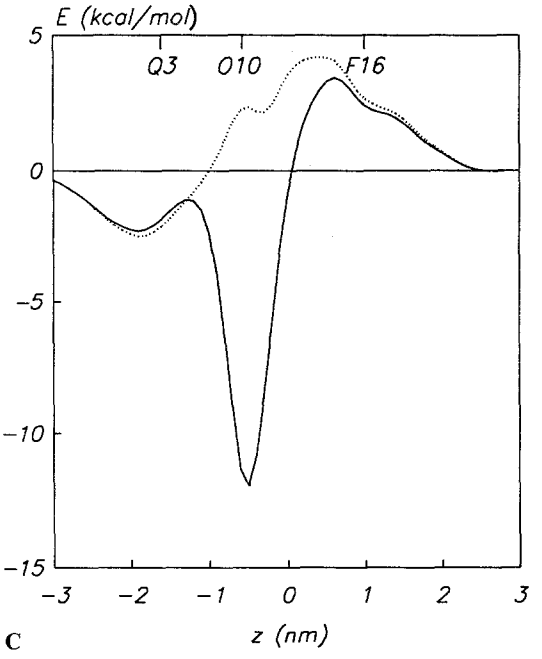

C

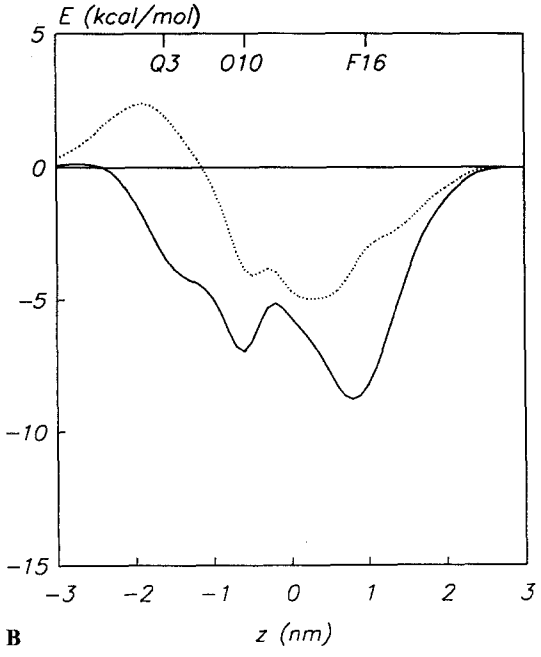

B

Fig. 5. (**A**) Comparison of conformations A, B and C of the Zrv-IIB monomer. The differences between these conformations are in the sidechains of Q3 and O10, and in the C-terminal hydroxyl group (F16-OH), which are highlighted using bold lines. (**B**) K^+ ion interaction energy profiles for $N=6$ helix bundles made up from monomers in conformation A (dotted line) vs. conformation B (solid line). The positions on z of the Cα atoms of residues Q3, O10 and F16 are indicated. (**C**) Cl^- ion interaction energy profiles for $N=6$ helix bundles made up from monomers in conformation A (dotted line) vs. conformation C (solid line)

sidechain was performed, and a lower energy conformation of Q3 selected. The change in conformation was from $\chi_1 = +66°$ (in the absence of the ion) to $-45°$ (in its presence), and from $\chi_2 = +29°$ to $+120°$. The change in conformation obtained with the K^+ ion adjacent to the hydroxyl of O10 was minor, with $\chi = C\beta-C\gamma-C\gamma-H\gamma$ changing from $+157°$ to $+150°$. A more substantial change occurred at the C-terminal hydroxyl, with $\chi =$ Cα–C–O–H changing from $-128°$ to $+20°$. Note that both of the latter changes only involve the terminal hydrogen atom of a hydroxyl group. These changes are shown in Fig. 5A. Conformation A is that before the above changes, whereas conformation B is that after the changes in the presence of K^+. (Note that the helix bundle models discussed in the previous section contained monomers in conformation B.) It is evident that the major difference between A and B is that the sidechain amide oxygen of Q3 is directed towards the centre of the pore in B. At the C-terminus the F16-OH hydrogen atom of B is directed away from the central pore.

An alternative conformation, conformation C, has been defined by performing conformational searches in the presence of a Cl^- ion. As before, the starting conformation was A, i.e. that based on the Zrv-Leu crystal structure. The conformation of sidechain Q3 was left unaltered. The positions of the hydroxyl hydrogens of O10 and F16-OH were changed via optimization in the presence of an adjacent Cl^- ion. This resulted in χ_1 and χ_2

values (as defined above) of $-70°$ and $-155°$ respectively. In both cases the hydrogen atom of the hydroxyl group was thus directed towards the Cl^- ion.

Channel-K^+ ion interactions

Conformations A and B of the Zrv-IIB monomer have been compared with respect to their K^+ interaction energy profiles for $N=6$ bundle models (Fig. 5 B). As the K^+ ion is translated along the z-axis from the N-terminus ($z=-1.8$ nm) to the C-terminus ($z=+1.0$ nm) of the conformation A bundle, there is an energy maximum in the region of the Q3 sidechain followed by a minimum close to O10 and a broad minimum at the C-terminus. Measurement of K^+–O and K^+–H closest approach distances (Table 2) suggests that the N-terminal maximum corresponds to an unfavourable interaction of the ion with the amide of Q3 in conformation A. In conformation B, the Oε:3 atom is closer to the K^+ ion. Inspection of the profile for conformation B reveals that the maximum close to Q3 is replaced by a shoulder representing favourable Q3-K^+ interactions. Also, the two other minima are deepened, reflecting the movement of the hydroxyl groups hydrogens away from the K^+ ion (Table 2). Overall, these calculations demonstrate that relatively small changes in sidechain conformations may optimize interactions with a permeant cation as it passes through the channel. Models based upon conformation B were used for all further calculations of K^+ ion profiles.

K^+ ion interaction energy profiles have been compared for helix bundle models with $N=4$, 5 and 6 monomers per helix. Before discussing these further, mention should be made of the helix bundle model for $N=4$. All other helix bundle models were generated with an interhelix separation of $R=0.95$ nm. In the case of the $N=4$ bundle model, this R value resulted in a "closed" channel. The corresponding interaction energy profiles (not shown) revealed a van der Waals barrier to translation of a K^+ ion along the central pore axis at ca. $z=-0.4$ nm, resulting from steric conflict between the ion and the Cβ atoms of the O10 residues. Conductance data (Balaram et al. 1992) suggest that Zrv-IIB channels do indeed open to an $N=4$ level, albeit infrequently. "Opening" the $N=4$ channel via sidechain conformational changes was not possible and so the effect of changing the inter-helix separation was investigated. Increasing R to 1.025 nm (i.e. an increase of 0.075 nm) removed the van der Waals energy barrier at $z=-0.4$ nm whilst still permitting formation of the inter-monomer hydrogen bond. This model for the $N=4$ bundle was therefore used in channel-ion and channel-water interaction energy profile calculations, and in monomer-monomer interaction energy calculations (see above).

Interaction energy profiles for $N=4$, 5 and 6 helix bundle models are shown in Fig. 6 A. All three profiles show minima at $z=-0.14$, -0.6 and $+0.9$ nm. These correspond to interactions between the K^+ ion and residues Q3, O10 and the C-terminal hydroxyl respectively. The K^+–O closest approach distances are given in Table 3. It is evident that although the closest approach is to the Oγ atom of O10, the strongest interaction is at the C-termini of the helices. This is because, in addition to O:16-K^+ interactions, K^+ interacts favourably with the C-terminal component of the helix dipoles. The $N=4$ profile shows a maximum at $z=-0.4$ nm, corresponding to the Cβ:10-K^+ close approach discussed above. It also shows an additional, small, minimum at $z=0$ nm. As will be discussed in more detail below, this reflects a favourable interaction between the K^+ ion and the carbonyl oxygen of residue 10.

In the above calculations, the K^+ ion is constrained to lie on the central pore (i.e. z-) axis. The effect of allowing the ion to move within the xy-plane whilst z remains fixed has also been explored. For each value of z, a grid of xy locations was explored, searching for the lowest channel-ion interaction energy. (Note that the size of this search was reduced by the N-fold symmetry of the channel.) For each z value, the xy coordinates and interaction energy at the minimum were stored. Figure 6 B shows the resultant interaction energy profile for such calculations using an $N=6$ bundle model. Similar results were ob-

Table 2. Ion-O and ion-H closest approach distances in $N=6$ bundle models: comparison of conformations A, B and C

Conformation	Ion	Atom	d/nm
A	K^+ or Cl^-	Oε:3	1.24
		Hε:3	0.95
		Oγ:10	0.56
		Hγ:10	0.59
		O:16	0.77
		H:16	0.67
B	K^+	Oε:3	0.82
		Hε:3	0.86
		Oγ:10	0.56
		Hγ:10	0.62
		O:16	0.77
		H:16	0.85
C	Cl^-	Oε:3	1.24
		Hε:3	0.95
		Oγ:10	0.56
		Hγ:10	0.47
		O:16	0.77
		H:16	0.67

Table 3. K^+–O and Cl^-–H distances: $N=4$, 5 and 6 bundle models

N			
	d(Oε:3-K^+)/nm	d(Oγ:10-K^+)/nm	d(O:16-K^+)/nm
4	0.60	0.37	0.55
5	0.68	0.42	0.65
6	0.82	0.56	0.77
	d(Hε:3-Cl^-)/nm	d(Hγ:10-Cl^-)/nm	d(H:16-Cl^-)/nm
4	0.75	0.29	0.45
5	0.80	0.33	0.55
6	0.95	0.47	0.67

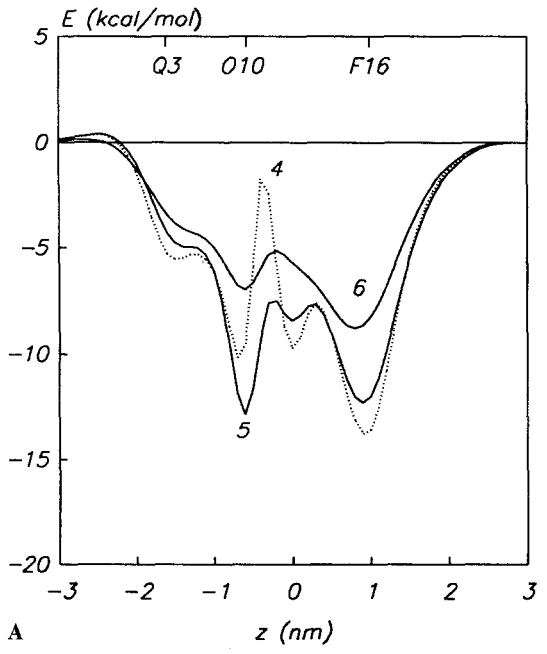

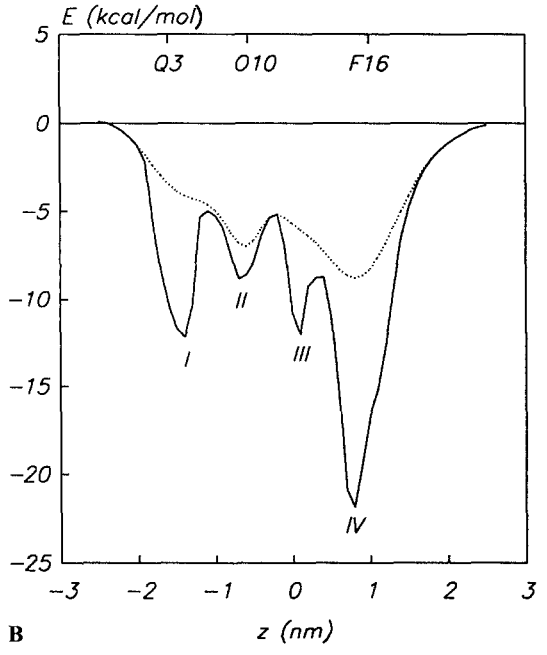

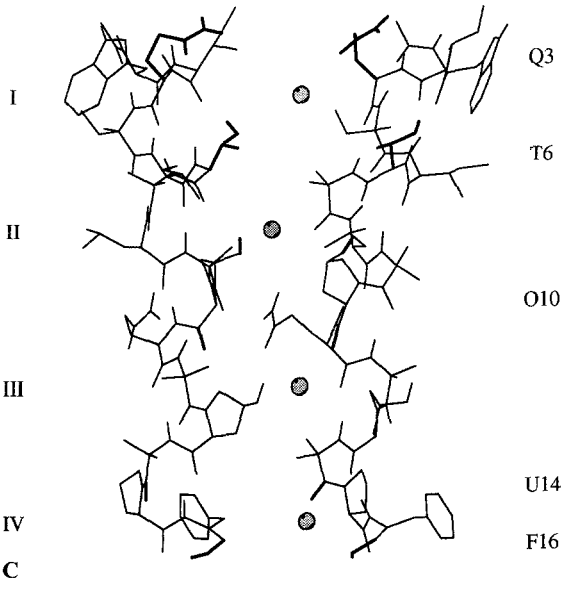

Fig. 6. (**A**) K^+ interaction energy profiles for $N=4$, 5 and 6 Zrv-IIB helix bundles. (**B**) Effect on the $N=6$ K^+ ion interaction profile of allowing the ion to move within the xy-plane for each position on z (see text for details). The dotted line gives the interaction profile when the ion is constrained to remain on z as in (**A**), the solid line the profile when it is free to move within the xy-plane. (**C**) K^+ ion interaction "sites" corresponding to the four minima (I to IV) labelled in the profile shown in (**B**). For clarity, only two monomers are shown. The view is from the centre of the pore, down an axis perpendicular to the monomer-monomer interface. For each "site" of the K^+ ion the closest approach to the channel is shown via a broken line, with the corresponding moiety of the peptide in bold

tained for $N=4$ and 5 models (not shown). Four distinct energy minima are seen – labelled I to IV. The corresponding K^+-O closest approach distances for these four "sites" are listed in Table 4. It can be seen that in all four cases, the interactions correspond to those discussed above in which the ion was constrained to lie on the central axis, but that the $O-K^+$ separations are considerably shorter. At site I, in addition to the interaction with Oε:3, there is a more distant interaction (0.51 nm) of K^+ with Oγ:6. The sidechain of T6 is hydrogen bonded back to the mainchain at O:2, thus exposing the Oγ:6 atom. Site III, at which the ion interacts with O:10, corresponds to the minor energy minimum seen in the $N=4$ and 5 profiles when the K^+ was constrained to lie on the z-axis.

The positions of the four sites in relation to the overall channel structure are shown in Fig. 6C. These calculations reveal that there are multiple locations for channel-cation interactions on the lining of the pore.

Channel-Cl^- ion interactions

The effect of changing the monomer conformation from A to C has been investigated with respect to the Cl^- ion interaction energy profile for $N=6$ helix bundle models (Fig. 5C). For a bundle of made up of conformation A monomers there is an energy minimum in the vicinity of the Q3 sidechains followed by maxima in the region of

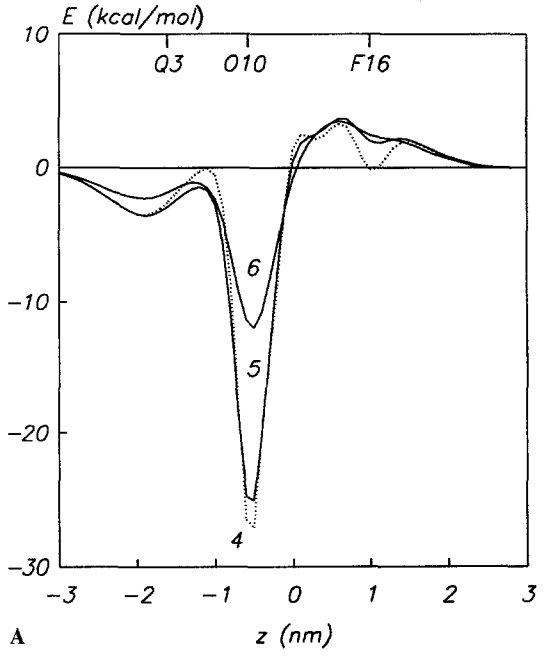

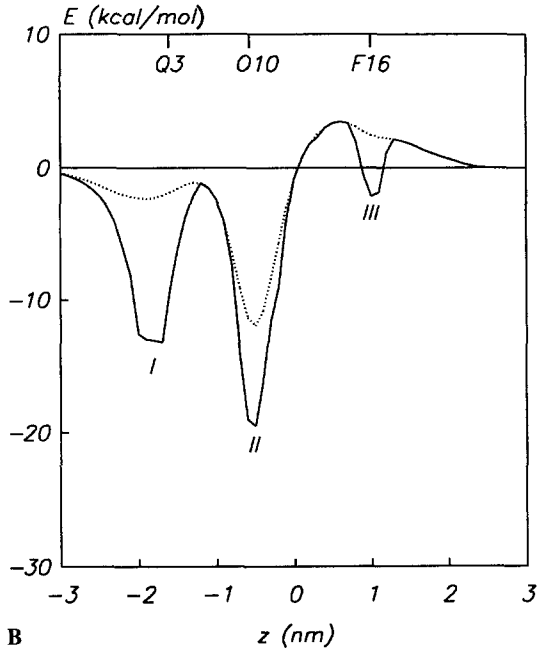

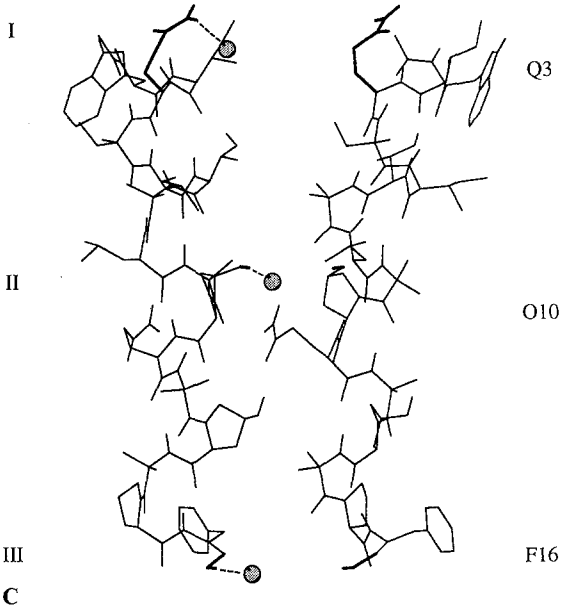

Fig. 7. (**A**) Cl^- ion interaction energy profiles for $N=4$, 5 and 6 Zrv-IIB helix bundles, with the monomers in conformation C. (**B**) Comparison of Cl^- ion profiles for the $N=6$ bundle model with the ion constrained to lie on the z-axis (dotted line) vs. free to move within the xy-plane for each value of z (solid line). (**C**) Cl^- ion interaction "sites" corresponding to the three minima (I to III) in the profile shown in (**B**). Two monomers are shown, viewed down an axis perpendicular to their interface. The broken lines indicate the closest approaches of the ion and the bold lines the residues involved in these interactions

O10 and at the C-termini of the helices. Inspection of closest approach distances (Table 2) reveals that the maxima are due to unfavourable interactions of the anion with the Oγ:10 and O:16 atoms respectively. In a conformation C bundle the hydroxyl hydrogens, Hγ:10, of O10 approach the Cl^- ion more closely. This converts the central maximum to an energy minimum. There is also some small reduction of the C-terminal maximum. Thus movement of the terminal hydrogens of hydroxyl groups of only one residue per monomer optimizes interactions with a permeant anion.

Cl^- ion interaction profiles have been evaluated for $N=4$, 5 and 6 Zrv-IIB models with the monomers in conformation C (Fig. 7A). As for the K^+ ion profiles, the $N=4$ model was generated with an interhelix separation of $R=1.025$ nm, whereas all other models employed $R=0.95$ nm, because for the tetrameric bundle the lower value of R resulted in a "closed" channel. The profiles for all three N values exhibit minima at $z=-1.9$ and -0.5 nm. These correspond to interactions of the anion with Hε:3 and Hγ:10 respectively (Table 3). All three profiles also exhibit maxima at $z=+0.6$ nm, corresponding to unfavourable interactions between the anion and the C-terminal dipoles of the helices. For the $N=4$ and 5 models, this interaction is somewhat counteracted by a favourable interaction with H:16 of the C-terminal hydroxyl group, resulting in minor energy minima at $z=+1.0$ nm. Overall, it is clear that the principal interac-

Table 4. K^+–O and Cl^-–H distances: $N=6$ bundle models, ions free to move in the xy-plane

Probe	Site	Atom	d/nm
K^+	I	Oε:3	0.30
	II	Oγ:10	0.32
	III	O:10	0.28
	IV	O:14	0.34
		O:16	0.30
Cl^-	I	Hε:3	0.24
	II	Hγ:10	0.22
	III	H:16	0.23

tion is with an annulus of hydrogen atoms around the Cl^- ion provided by the hydroxyls of the O10 residues.

The effect on the Cl^- ion profile of allowing the anion to move within the xy-plane for each value of z has been explored (Fig. 7B) for the $N=6$ model. Comparison with the corresponding profile generated when Cl^- was constrained to lie on the z-axis reveals that the main change is a deepening of the minimum corresponding to interactions with the Q3 sidechains. Three interaction "sites" are thus defined. Inspection of the closest approach distances at these sites (Table 4) reveals that in each case there is a close interaction between the anion and a polar hydrogen, as may clearly be seen in Fig. 7C. Note that the favourable interactions at site III partially compensate for the unfavourable interactions of the anion with the C-termini of the helices.

Channel-water interactions

To a first approximation, ion movements through the higher conductance Zrv-IIB channels may be treated as a diffusion-like process (Balaram et al. 1992). This suggests that water molecules may interact favourably with the lining of the central pore. Furthermore, an underlying assumption in construction of helix bundle models is that the central pore is hydrophilic. It is thus of some importance to evaluate possible interactions of water molecules with Zrv-IIB channel models.

Interaction energy profiles for water molecules translated along z have been evaluated for Zrv-IIB models with monomers in conformations A, B and C. Those for the $N=6$ models are shown in Fig. 8A. To some extent these profiles reflect the hydrophilic surface map presented earlier. Thus, each profile shows three broad minima – one in the region of the N-termini of the helices, one in the region of the C-termini and a central minimum close to residues 10 and 11. This suggests that water molecules may interact with either mouth of the channel and also with the centre of the channel. More detailed inspection of the profiles reveals that for conformation A bundles, the deepest minimum is in the region of residue O10, for conformation B bundles it is at the C-terminus and for conformation C bundles it is close to residue Q11. Thus the interaction energy profile for water is sensitive to the exact conformation of the hydrophilic sidechains lining the pore.

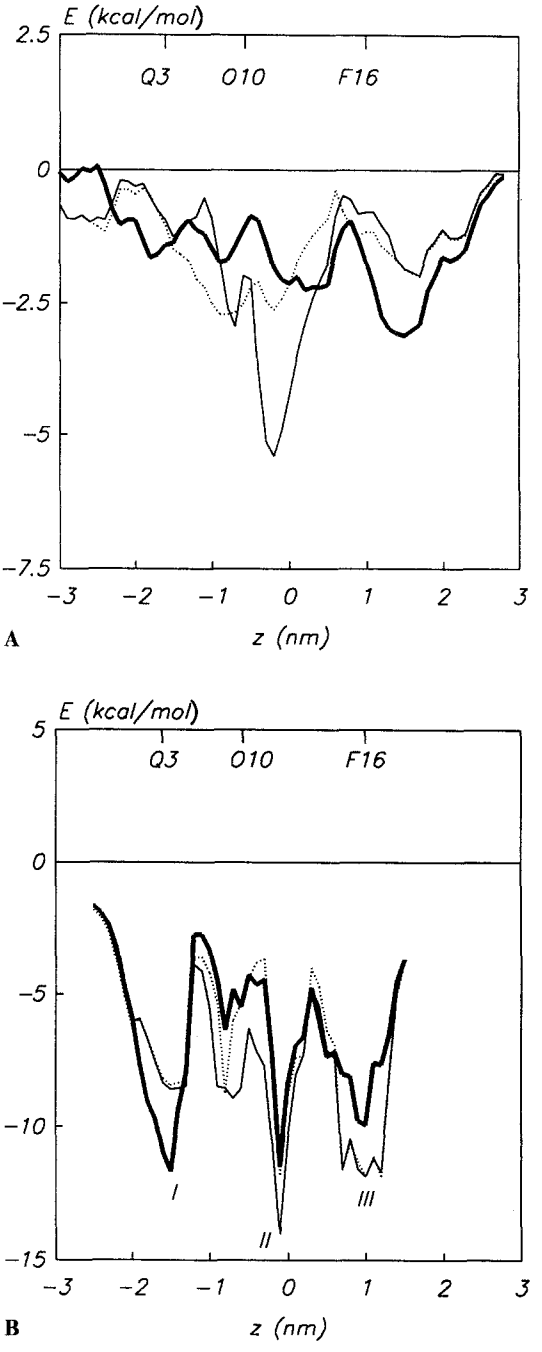

Fig. 8. (A) Water molecule interaction energy profiles for $N=6$ Zrv-IIB helix bundle models with the monomers in conformation A (dotted line), B (bold line) and C (thin line). In each case a water molecular was translated along z, with an energy minimization at each z value in order to optimize the positions of the hydrogen atoms (see text). (B) Water profiles for which the water molecule was free to move within the xy-plane. Profiles for $N=6$ bundle models with the monomers in conformation A (dotted line), B (bold line) and C (thin line) are compared. The minima discussed in the text (I to III) are labelled

Similarities between the profiles for the three different monomer conformations are greater if the water molecule is allowed to move within the xy-plane for each value of z (Fig. 8B). In this case three main interaction "sites", I, II and III, are observed. These correspond to: (a) site I,

Table 5. Water-channel distances: $N=6$ bundle models, water molecules free to move in the xy-plane

Conformation	Site	Probe	Atom	d/nm
A and C	I	O_W	Hγ:6	0.30
		H_W	O:2	0.22
			Oγ:6	0.27
	II	O_W	Hε:11	0.21*
		H_W	O:10	0.22
	III	H_{W1}	O:14	0.22
		H_{W2}	O:15	0.25
			O:16	0.25
B	I	O_W	Hε:3	0.24*
	II	O_W	Hε:11	0.22*
	III	O_W	H:16	0.25
		H_W	O:16	0.23

(A * indicates that a hydrogen bond is formed)

interactions with the sidechains of Q3 and/or T6; (b) site II, interactions with O:10 and/or the sidechain of Q11; and (c) site III, interactions with O:14, O:15 and/or O:16 (see Table 5). Note that all of these interactions, with the exception of that involving the sidechain of Q11, correspond to peptide-water hydrogen bonds present within the Zrv-Leu crystal structure (Karle et al. 1991). Interactions are very similar for monomer conformations A and C. The only real difference is that the profile for conformation C shows a more pronounced (minor) minimum in the region of residue O10. In certain cases it would appear that a channel-water hydrogen bond may be formed: e.g. from Hε:3 to the water oxygen (O_W) for site I (monomer conformation B); and from Hε:11 to O_W for site III (all three monomer conformations). Overall, these results confirm that water molecules interact favourably with the lining of the channel at several different locations. It should be remembered that each "site" described above is present for each of the N monomers in bundle.

Discussion

Zrv-IIB monomer

It is important to consider whether it is reasonable to model the Zrv-IIB monomer structure on the basis of the Zrv-Leu crystal structure. As noted by Karle et al. (1991), the backbone conformation of Zrv-Leu is almost identical to that of a synthetic apolar zervamicin (Zrv-A1-16; Karle et al. 1987). Furthermore, the conformations of Zrv-Leu crystallised from methanol/water and from ethylene glycol/ethanol are extremely similar. As Zrv-A1-16 resembles Zrv-IIB in having a tryptophan at position 1, this supports the proposal that the same backbone conformation will be found in Zrv-IIB. The conformation of the W1 sidechain in the Zrv-IIB model, obtained by a conformational search about χ_1 and χ_2 differs from that in Zrv-A1-16. However, the results of our subsequent calculations are not too sensitive to the W1 conformation. One remaining concern is whether the conformation of Zrv will be the same in a bilayer environment. In this respect, the similarity between the structures of alamethicin as determined by NMR (in methanol; Esposito et al. 1987) and in crystals (Fox and Richards 1982) provides reassurance.

The amphipathic nature of Zrv-IIB is evident from the hydrophilic surface plot. This method of analysis has been applied to a number of channel-forming peptides (e.g. alamethicin, melittin, *S. aureus* δ-toxin) and has proved a valuable tool in the construction of helix bundle models (Kerr and Sansom 1992). Three hydrophilic patches on the surface of the monomer were identified – at the N- and C-termini, and in the vicinity of the polar sidechains of O10 and Q11. This is in reasonable agreement with the patterns of hydrogen bonding to water molecules in the Zrv-Leu crystal structure, namely: (a) at the N-terminus, atoms O:3, Oε:3 and Hε:3; (b) at the C-terminus, atoms O:14, O:15 and H:16; and (c) in the centre, atoms O:10, O:11 and Oδ:13.

Zrv-IIB helix bundles

The results of electrical measurements from channels in planar bilayers (Balaram et al. 1992) place constraints upon possible helix bundle models for Zrv-IIB. An asymmetric current-voltage relationship is seen if a bilayer is exposed to Zrv-IIB on one face only. This is best explained by a model in which the helices run approximately parallel, rather than anti-parallel, to one another. The sequence of multiple conductance levels observed suggests that bundles which are approximately circular in cross-section, i.e. possess rotational symmetry, are formed for $N=4$ to 8 monomers/bundle. For higher N values the bundles are distorted and the rotational symmetry is lost. These constraints considerably reduced the number of models which had to be considered. The major difficulty lay in determining a suitable value of θ for bundle construction. This was considerably aided by the secondary $\langle E \rangle$ vs. ϕ plot derived from the hydrophilic surface map. Whilst not proposing that the resultant model is a definitive representation of the structure of Zrv-IIB channels in bilayers, it is sufficiently accurate to merit the subsequent analysis.

An important feature of the channel model is stabilization of the helix bundles by inter-monomer hydrogen bonds (O13(B) → Q11(A)). This is comparable to the proposals of Nagaraj and Balaram (1981) and of Fox and Richards (1982) for stabilization of alamethicin helix bundles by inter-monomer hydrogen bonding. It also should be compared with the presence of an O10 → Q11 hydrogen bond between antiparallel helices in Zrv-Leu crystals. An O13(B) → Q11(A) hydrogen bond is found in Zrv-IIB bundles from $N=4$ to 8, and the monomer-monomer interaction energy is approximately independent of N. This is in agreement with the results of analysis of gating kinetics of single Zrv-IIB channels (Balaram et al. 1992) which suggest that helix bundles are of approximately equal stability for $N=4$ to 8. For values of $N>8$ the experimental bundle stability becomes dependent on N.

However, the corresponding bundle models were not constructed as analysis of conductance levels suggests higher N bundles may not exhibit cyclic symmetry. An apolar analogue, Zrv-A1-16, is unable to form intermonomer hydrogen bonds, and although it forms channels in lipid bilayers, only two conductance levels are seen, rather than the regular succession on conductance levels observed with Zrv-IIB, Zrv-Leu, alamethicin, and other peptaibols. Together, these complementary approaches provide good evidence for a role of hydrogen bonding in stabilization of peptaibol helix bundles. This also is consistent with the proposed role of intermonomer hydrogen bonds. It is possible that such a role may be more generally applicable to CFPs, and to ion channel proteins. Spach et al. (1985) discussed a general model for CFPs in which hydrophobic and hydrophilic faces of a helix are separated by two "border" regions which contain small sidechains in order to facilitate intermonomer packing. Introduction of hydrogen-bonding pairs of sidechains into the border regions would result in greater stability of helix bundles. For example, it is possible that channels formed by the leucine- and serine-containing 21 residue peptides designed by Lear et al. (1988) may be stabilized in this manner.

It is useful to examine which aspects of Zrv-IIB channels are not encompassed in the current model. The helix bundle model provides an explanation of the *open channel* properties of Zrv-IIB. It does not attempt to explain the gating properties of Zrv-IIB channels. Thus, we have addressed neither the complex problem of the nature of the voltage dependent step in Zrv-IIB channel formation, nor the kinetics of uptake and release of monomers from the helix bundle. The latter process appears to be extremely sensitive to changes in peptaibol structure in that, for example, Zrv-Leu exhibits more rapid switching between adjacent conductance levels than does Zrv-IIB.

Sidechain conformations

An important element of this study is the importance of polar sidechain conformations in determining channel-ion interactions. Such considerations fall into two classes: (a) the position of the terminal hydrogen atoms of the hydroxyl groups of O10 and of F16-OH, as determined by rotation about C–O bonds; and (b) the conformation of the sidechain of residue Q3.

With respect to the positions of the hydroxyl hydrogens, previous modelling studies (Sansom 1992 b) indicated that in simplified models of the central M2 helix bundle of the nicotinic acetylcholine receptor channel-ion interactions were strongly dependent upon the χ_2 ($=C\alpha-C\beta-O\gamma-H\gamma$) values of serine and threonine sidechains. The χ_2 values adopted were determined by electrostatic interactions between sidechain hydroxyl groups and permeant ions. Neutron diffraction studies of hydroxyl hydrogen conformations in trypsin (Kossiakoff et al. 1990) have revealed that, in situations where there is an incompatibility between steric and electrostatic criteria, the latter are dominant in determining $H\gamma$ positions. Similar conclusions have been obtained by Brünger and Karplus (1988) on the basis of empirical energy calculations.

The "optimization" procedure used in order to determine hydroxyl group conformations in the presence of permeant ions is an approximation which enables interaction energy profiles to be calculated using treating the channel model as a rigid body. An alternative procedure is to translate the ion along z, and for each position of the ion to perform an energy minimization in which sidechain atoms are allowed to move whilst mainchain coordinates are fixed. This was used by e.g. Furois-Corbin and Pullman (1991) in their study of the nicotinic acetylcholine receptor. A comparable approach has been evaluated (Sansom, unpublished results) on both Zrv-IIB and on M2 helix bundle models. Profiles thus obtained were similar to those derived via the "optimization" procedure used in the current study.

The conformational changes which have been explored with respect to Q3 sidechains are more extensive. Some support for such changes comes from the crystal structure of Zrv-Leu, in which the amide group of Q3 is relatively mobile in all three crystal forms (Karle et al. 1991). It is useful to consider possible effects of electrostatic fields upon the conformation of Q3, in particular reorientation of the terminal amide dipole within such fields. The dipole moment of the amide group is of the order of 4.2 D. The field due to a transbilayer voltage of 100 mV would be of the order of 4×10^7 V m^{-1}. The maximum difference in potential energy between two orientations of the amide dipole with respect to such a field is ca. 0.4 kT, i.e. considerably less than the mean thermal energy of the molecule. Hence, the transbilayer potential is insufficient to determine the conformation of Q3, or of other glutamine sidechains, in Zrv-IIB channels. This suggests that changes in sidechain orientation are unlikely to constitute the primary event in voltage-dependent activation of peptaibol channels. However, e.g. the electrostatic field at a distance of 1 nm from a K^+ ion (for $\varepsilon = 2$) is such that the maximum difference in potential energies between two orientations of the amide dipole is ca. 5 kT. Thus it is plausible to suggest that the conformation of Q3 may alter in response to the local electrostatic field around a permeant ion. One must also consider the timescale of such conformational changes in relation to the mean dwell time of an ion within the channel. A conductance of 1 ns at a membrane potential of 100 mV results in a current of 100 pA, corresponding to a net flux of ca. 6×10^8 ion s^{-1}. Thus the mean dwell time of an ion in the channel is of the order of 2 ns. It is more difficult to obtain an estimate for the time constant of sidechain conformational changes. For example, Hoch et al. (1985) suggest a figure of ca. 10^{11} s^{-1} (or less) as the frequency of conformational fluctuations arising from transitions between sidechain rotamers. In a molecular dynamics simulation of bovine pancreatic trypsin inhibitor they observed conformational transitions of an arginine and of a glutamate sidechain with time constants of the order of 10 ps. This suggests that the time constant for Q3 conformational transitions may be two or three orders of magnitude smaller than the mean dwell time of an ion within the channel. Therefore, there is sufficient time for sidechain

conformational changes to occur in response to the local electrostatic fields generated by permeant ions.

Interaction energy profiles

As noted earlier in this paper, in estimating interaction energy profiles it is not our intention to estimate permeation profiles for ions or water molecules moving through the channel. Rather, profiles have been evaluated in order to locate possible interaction sites between the channel and the probe ion/molecule.

The interaction profiles for both an anion and a cation reveal multiple sites at which favourable interactions may occur. With respect to K^+, reorientation of Q3 is important in allowing favourable interactions to develop at the N-terminal mouth of the pore. For Cl^-, reorientation of the hydroxyl hydrogens of O10 is necessary to enable favourable interactions to ensue once the anion has entered the pore. In both cases, more favourable interactions are possible if the ion moves away from the central pore axis. Interaction energy profiles also suggest that water molecules may bind to the lining of the pore at both the N- and C-terminal mouths and also in the central region. In particular, residues Q3 and Q11 may form hydrogen bonds to water molecules within the pore.

Electrical measurements show that the single channel conductances of $N=4$ to 8 helix bundles are in agreement with the predictions of a simple diffusion model for ion movement through the channel. Consequently it is likely that ions move through the channel in a hydrated form (at least for $N \geq 5$) and that the channel does not select between anions and cations. Therefore the observation that Zrv-IIB channels may interact favourably with anions, cations or water molecules is important in that it suggests that conformational flexibility of polar sidechains enables the channel lining to mimic an aqueous environment. This is similar to the role proposed (Sansom 1992 b) for serine and threonine sidechains lining the central pore of channels of members of the nicotinic receptor superfamily of channel proteins.

Overall, the studies described in this paper illustrate that substantial progress can be made towards understanding the relationship between ion channel structure and function when crystallographic information is available upon which to base helix bundle models. Current studies are directed towards improving the methodology for modelling, and towards extending its application to a wide range of CFPs and ion channel proteins.

Acknowledgements. This work was supported by grants from the Wellcome Trust, and the SERC, UK (to MSPS), from the Department of Science and Technology, India (to PB) and from the National Institutes of Health (grant number GM30902) and the Office of Naval Research, USA (to ILK).

References

Agarwalla S, Mellor IR, Sansom MSP, Karle IL, Flippen-Anderson JL, Uma K, Krishna K, Sukumar M, Balaram P (1992) Zervamicins, a structurally characterised peptide model for membrane ion channels. Biochem Biophys Res Commun 186:8–15

Balaram P, Sukumar M, Krishna K, Mellor IR, Sansom MSP (1992) The properties of ion channels formed by zervamicins. Eur Biophys J 21:117–128

Boheim G, Gelfert S, Jung G, Menestrina G (1987) α-Helical ion channels reconstituted into planar bilayers. In: Yagi K, Pullman B (eds) Ion transport through membranes. Academic Press, Tokyo, pp 131–145

Brooks BR, Bruccoleri RE, Olafson BD, States DJ, Swaminathan S, Karplus M (1983) CHARMM: a program for macromolecular energy, minimization, and dynamics calculations. J Comp Chem 4:187–217

Brünger AT, Karplus M (1988) Polar hydrogen positions in proteins: empirical energy placement and neutron diffraction comparison. Proteins: Struct Func Genet 4:148–156

Esposito G, Carver JA, Boyd J, Campbell ID (1987) High resolution ^{1}H NMR study of the solution structure of alamethicin. Biochem 26:1043–1050

Fox RO, Richards FM (1982) A voltage-gated ion channel model inferred from the crystal strcture of alamethicin at 1.5 Å resolution. Nature 300:325–330

Furois-Corbin S, Pullman A (1986) Theoretical study of the packing of α-helices by energy minimization: effect of the length of the helices on the packing energy and on the optimal configuration of a pair. Chem Phys Lett 123:305–310

Furois-Corbin S, Pullman A (1991) The effect of point mutations on energy profiles in a model of the nicotinic acetylcholine receptor (AChR) channel. Biophys Chem 39:153–159

Goodford PJ (1985) A computational procedure for determining energetically favorable binding sites on biologically important macromolecules. J Med Chem 28:849–857

Hall JE, Vodyanoy I, Balasubramanian TM, Marshall GR (1984) Alamethicin: a rich model for channel behaviour. Biophys J 45:233–247

Hoch JC, Dobson CM, Karplus M (1985) Vicinal coupling constants and protein dynamics. Biochem 24:3831–3841

Hol WG, von Duijen PT, Berendsen HJC (1978) The α-helix dipole and the properties of proteins. Nature 273:443–446

Janin J, Wodak S, Levitt M, Maigret B (1978) Conformations of amino acid sidechains in proteins. J Mol Biol 125:357–386

Jeffrey GA, Saenger W (1991) Hydrogen bonding in biological structures. Springer, Berlin Heidelberg New York

Karle IL, Flippen-Andersen J, Agarwalla S, Balaram P (1991) Crystal structure of Leu-zervamicin, a membrane ion channel peptide. Implications for gating mechanisms. Proc Natl Acad Sci USA 88:5307–5311

Karle IL, Flippen-Andersen J, Sukumar M, Balaram P (1987) Conformation of a 16-residue zervamicin IIA analog peptide containing 3 different structural features: 3_{10}-helix, α-helix and β-bend ribbon. Proc Natl Acad Sci USA 84:5087–5091

Kerr ID, Sansom MSP (1992) Hydrophilic surface maps of α-helical channel-forming peptides (manuscript in preparation)

Kossiakoff AA, Shpungin J, Sintchak MD (1990) Hydroxyl hydrogen conformations in trypsin determined by the neutron diffraction solvent difference map method: relative importance of steric and electrostatic factors in defining hydrogen-bonding geometries. Proc Natl Acad Sci USA 87:4468–4472

Kraulis PJ (1991) MOLSCRIPT: a program to produce both detailed and schematic plots of protein structures. J Appl Cryst 24:946–950

Krishna K, Sukumar M, Balaram P (1990) Structural chemistry and membrane modifying activity of the fungal polypeptides zervamicins, antiamoebins and efrapeptins. Pure Appl Chem 62:1417–1420

Lear JD, Wasserman ZR, DeGrado WF (1988) Synthetic amphiphilic peptide models for protein ion channels. Science 240:1177–1181

Mathew MK, Balaram P (1983) A helix dipole model for alamethicin and related transmembrane channels. FEBS Lett 157:1–5

Nagaraj R, Balaram P (1981) Alamethicin, a transmembrane channel. Acc Chem Res 14:356–362

Nilges M, Brünger AT (1991) Automated modeling of coiled coils: application to the GCN4 dimerization region. Prot Engineer 4:649–659

Rinehart KL, Gaudioso LA, Moore ML, Pandey RC, Cok JC, Brber M, Sedgwick D, Bordoli RS, Tyler AN, Green BN (1981) Structures of eleven zervamicin and two emerimicin peptide antibiotics studied by fast atom bombardment mass spectroscopy. J Am Chem Soc 103:6517–6520

Sansom MSP (1991) The biophysics of peptide models of ion channels. Prog Biophys Mol Biol 55:139–235

Sansom MSP (1992a) Proline residues in transmembrane helices of channel and transport proteins: a molecular modelling study. Prot Engineer 5:53–60

Sansom MSP (1992b) An investigation of the role of serine and threonine sidechains in ion channel proteins. Eur Biophys J 21:281–298

Sansom MSP (1992c) Sidechain-ion interactions in ion channels: a molecular modelling study. Biochem Soc Trans 20:254

Sansom MSP, Kerr ID, Mellor IR (1991) Ion channels formed by amphipathic helical peptides – a molecular modelling study. Eur Biophys J 20:229–240

Schifffer M, Chang CH, Stevens FJ (1992) The functions of tryptophan residues in membrane proteins. Prot Engineer 5:213–214

Spach G, Merle Y, Molle G (1985) Peptide amphiphiles et canaux transmembranes. J Chim Phys 82:719–721

Toyoshima C, Unwin N (1990) Three-dimensional structure of the acetylcholine receptor by cryoelectron microscopy and helical image reconstruction. J Cell Biol 111:2623–2635